AIAC-2005-011

# PATH OPTIMIZATION OF FLAPPING AIRFOILS FOR MAXIMUM THRUST BASED ON UNSTEADY VISCOUS FLOW SOLUTIONS

Mustafa Kaya* and Ismail H. Tuncer†
Middle East Technical University
Ankara, Turkey

## ABSTRACT

The path of a flapping airfoil during upstroke and downstroke is optimized for maximum thrust and propulsive efficiency. Unsteady, low speed laminar flows are computed using a Navier-Stokes solver in a parallel computing environment based on domain decomposition. The periodic flapping motion of the airfoil is described by a combined plunge and pitching motions, and the phase shift between them. A gradient based algorithm is employed for optimization. Definition of the periodic flapping motion with a new parameter, flatness coefficient, $s$, provides high enhancement in the thrust generation. For high thrust, the airfoil stays at high effective angle of attack values for short durations.

## INTRODUCTION

Based on observations of flying birds and insects, and swimming fish, flapping wings have been recognized to be more efficient than conventional propellers for flights of very small scale vehicles, socalled microair vehicles (MAVs) with wing spans of $15\ cm$ or less. The current interest in the research and development community is to find the most energy efficient airfoil adaptation and flapping wing motion technologies capable of providing the required aerodynamic performance for a MAV flight.

Recent experimental and computational studies investigated the kinematics, dynamics and flow characteristics of flapping wings, and shed some light on the lift, drag and propulsive power considerations[9, 14]. Water tunnel flow visualization experiments on flapping airfoils conducted by Lai and Platzer[15] and Jones et al.[16] provide a considerable amount of information on the wake characteristics of thrust producing flapping airfoils. In their experiments, Anderson et al.[17] observed that the phase angle between pitch and plunge oscillations plays a significant role in maximizing the propulsive efficiency. NavierStokes computations performed by Tuncer et al.[19, 18, 11] and by Isogai et al.[13, 10] explore the effect of flow separation on the thrust generation and the propulsive efficiency of a single flapping airfoil in combined pitch and plunge oscillations.

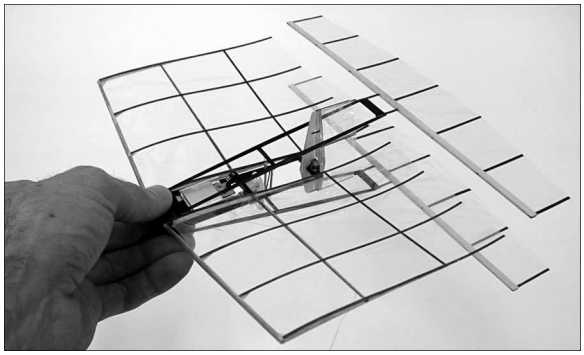

Figure 1: Flapping-wing MAV model(Jones and Platzer)

Jones and Platzer[6] recently demonstrated a radiocontrolled micro air vehicle propelled by flapping wings in a biplane configuration (Figure 1). The experimental and numerical studies by Jones et al.[6, 7, 8] and Platzer and Jones[12] on flappingwing propellers points at the gap between numerical flow solutions and the actual flight conditions over flapping wings.

Most recently, Kurtulus et al.[1] obtained optimum parameters to generate maximum lift during a flapping motion of an airfoil in hovering flight, by using numerical and analytical models. The wake structures and hydrodynamic performance of finite aspect-ratio flapping foils are explored by Dong et al.[2]. The results of their numerical simulations indicate that the wake topology of the relatively low aspect-ratio foils is significantly different from that observed for infinite/large aspect-ratio foils.

In our earlier studies[19, 11], the average thrust coefficient of a NACA0012 airfoil flapping sinusoidally in combined plunge and pitch was first obtained for a range of reduced frequencies and amplitudes of the flapping motion. The computational and experimental findings show that thrust generation and propulsive efficiency of flapping airfoils are closely connected to the flapping motion and flow parameters. In a later study[5], we employed a gradient based optimization of flapping motion parameters; flapping frequency, the amplitude of the pitch and plunge motions, and the phase shift between them to maximize the thrust and/or the propulsive efficiency of flapping airfoils.

*GRA in the Dept. of Aerospace Engineering, Email: mkaya@ae.metu.edu.tr
†Prof. in the Dept. of Aerospace Engineering, Email: tuncer@ae.metu.edu.tr

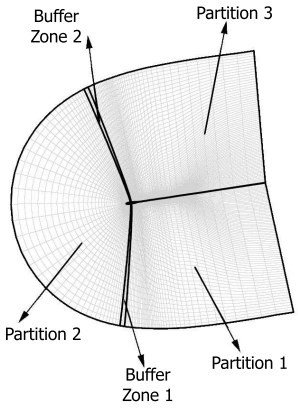


Figure 2: Domain decomposition with 3 partitions

In these studies, the periodic flapping motion is assumed to be sinusoidal, where the pitch and plunge positions are based on the projection of a vector rotating on a unit circle. It should be noted that the sinusoidal motion imposes the maximum plunge and pitch velocities at the mean plunge and pitch positions. In this study, the sinusoidal periodic motion is relaxed by replacing the unit circle with an ellipse, and introducing the flatness coefficient as the ratio of the axes of the ellipse. First, the thrust production of a flapping airfoil in plunge only is studied parametrically, and distinguishing features of the flatness coefficient are identified at a fixed frequency. Then, the optimization method developed earlier[4] is employed to optimize a linear combination of the thrust and the propulsive efficiency of an airfoil undergoing a combined plunge and pitch oscillations. The optimization variables are taken to be the pitch amplitude, $\alpha_0$, the phase shift between the pitch and plunge motions, $\phi$, and the plunge and pitch flatness coefficients, $s_h$ and $s_\alpha$. Unsteady flow solutions required to evaluate the gradients of the objective function by perturbation of the optimization variables are computed in parallel in a computer cluster.

## NUMERICAL METHOD

Unsteady viscous flowfields around a flapping airfoil are computed by solving the Navier-Stokes equations on a moving C-grid. Unsteady computations are performed in parallel based on domain decomposition (Figure 2). `PVM` message passing library routines are used in the parallel solution algorithm. The computed flowfields are analyzed in terms of aerodynamic loads, instantaneous distribution of flow variables, and unsteady particle traces.

The flapping motion of the airfoil is imposed by moving the airfoil and the computational grid around it. The flapping motion of the airfoil in plunge, $h$, and pitch, $\alpha$, is defined by

$$\begin{aligned} h &= -h_0 \frac{s_h \cos(\omega t)}{\sqrt{s_h^2 \cos^2(\omega t) + \sin^2(\omega t)}} \\ \alpha &= -\alpha_0 \frac{s_\alpha \cos(\omega t + \phi)}{\sqrt{s_\alpha^2 \cos^2(\omega t + \phi) + \sin^2(\omega t + \phi)}} \end{aligned} \quad (1)$$

where $s$ is the flatness coefficient which describes the elliptic path a rotation vector traces as shown in Figure 3. Note that for $s = 1$, the flapping motion becomes sinusoidal. Figure 4 shows the plunge position and the velocity of the periodic flapping motions as a function of flatness coefficient for the plunge motion, $s_h$. In the case $s_h = 0.25$, the plunge velocity is maximum in the vicinity of the minimum and maximum plunge positions, whereas, in the case $s_h \geq 1$, the plunge velocity reaches its maximum at the mean plunge position.

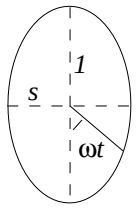


Figure 3: Definition of the periodic motion

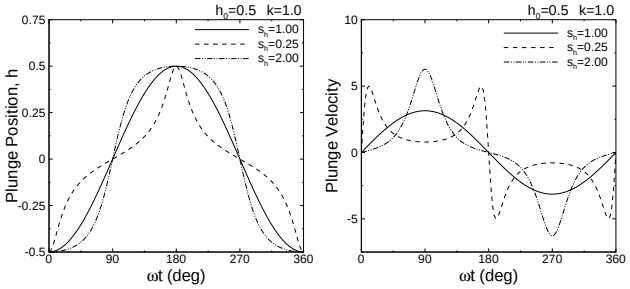


Figure 4: Plunge position and velocity as a function of $s_h$

### Optimization

Optimization process is simply performed marching along the direction of steepest ascent of an objective function, $O$. The direction of the steepest ascent is given by the gradient vector of the objective function: $\vec{\nabla} O(\vec{v}_n) = \frac{\partial O}{\partial V_1}\vec{v}_1 + \frac{\partial O}{\partial V_2}\vec{v}_2 + \cdots$, where $V_n$'s are the optimization variables of the objective function. The objective function in optimization step $k$ is taken as a linear combination of the average thrust, $C_t$, and the propulsive efficiency, $\eta$, over a flapping period. $\beta = 0$ sets the objective function to a normalized thrust coefficient:

$$\begin{aligned} O^k[C_t, \eta] &= (1-\beta)\frac{C_t}{C_t + \epsilon^{k-1}\left|\vec{\nabla} C_t \cdot \vec{D}^{k-1}\right|} \\ &\quad + \beta \frac{\eta}{\eta + \epsilon^{k-1}\left|\vec{\nabla}\eta \cdot \vec{D}^{k-1}\right|} \end{aligned} \quad (2)$$

where $\epsilon$ denotes the stepsize along the steepest ascent direction.

The components of the gradient vector is then evaluated numerically by computing the objective function for a small perturbation of the optimization variables one at a time. It should be noted that the evaluation of these vector components requires an unsteady flow computation over a few periods of the flapping motion until a periodic behavior is reached. Once the unit vector in the ascent direction is evaluated by $\vec{D} = \frac{\vec{\nabla} O}{|\vec{\nabla} O|}$, the step $\triangle \vec{V} = \epsilon \vec{D}$ is to be determined. Reference [4] suggests a way to predict the stepsize $\epsilon$ based on the gradients in the current and previous optimization steps.

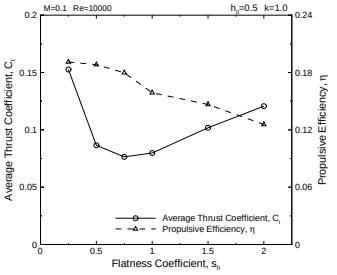


Figure 5: Thrust and efficiency for $s_h = 0.25 - 2.0$

### Parallel Computation

A coarse parallel algorithm based on domain decomposition is implemented in a master-worker paradigm. The computational C-grid is decomposed into overlapping subgrids (shown as partitions in Figure 2), and the solution on each subgrid is obtained in parallel. Intergrid boundary conditions at the overlapping boundaries (shown as buffer zones in Figure 2) are exchanged among subgrid processes. In addition, in the optimization process, the gradient vector components are evaluated in parallel. `PVM` (version 3.4.5) library routines are used for inter-process communication. Computations are performed in a PC cluster operating on Linux.

## RESULTS

In this work, the unsteady laminar flowfields are first computed at a low Mach number of $0.1$ and a Reynolds number of $10000$ for a parametric study in terms of flatness coefficient for flapping motions in plunge only. Optimization studies for combined plunge and pitch motions are then carried out. The optimization variables are chosen as the pitch amplitude, the phase shift between the pitch and plunge motions, and the plunge and pitch flatness coefficients. The reduced frequency of the periodic motion, $k \equiv \frac{\omega c}{U_\infty}$, and the plunge amplitude, $h_0$, are kept fixed at $k = 1$ and $h_0 = 0.5$ in both parametric and optimization studies. The corresponding unsteady flowfields are analyzed in terms of particle traces, the variation of the thrust/drag coefficient, and the average thrust and the propulsive efficiency.

### Parametric Study

The flatness coefficient of plunge, $s_h$ varies in the range $0.25 - 2.0$ (Figure 5). The figure shows the computed average thrust coefficients and propulsive efficiencies. It is observed that $s_h = 0.25$ case produces the highest thrust at the highest efficiency. The sinusoidal plunge motion and the flowfield for $s_h = 1.0$ is given in Figure 6. The characteristic leading edge vortices developing during the upstroke and the downstroke of the plunging motion, and their shedding into the wake are clearly observed. In Figure 7, the flowfield for $s_h = 2.0$ is given. In this case, the plunge velocities are higher at the mean plunge positions, and in a period, the airfoil stays longer at the minimum and maximum positions than that of the sinusoidal motion. The main features of the flow are the same as the previous case, except the leading edge vortices are observed to be stronger.

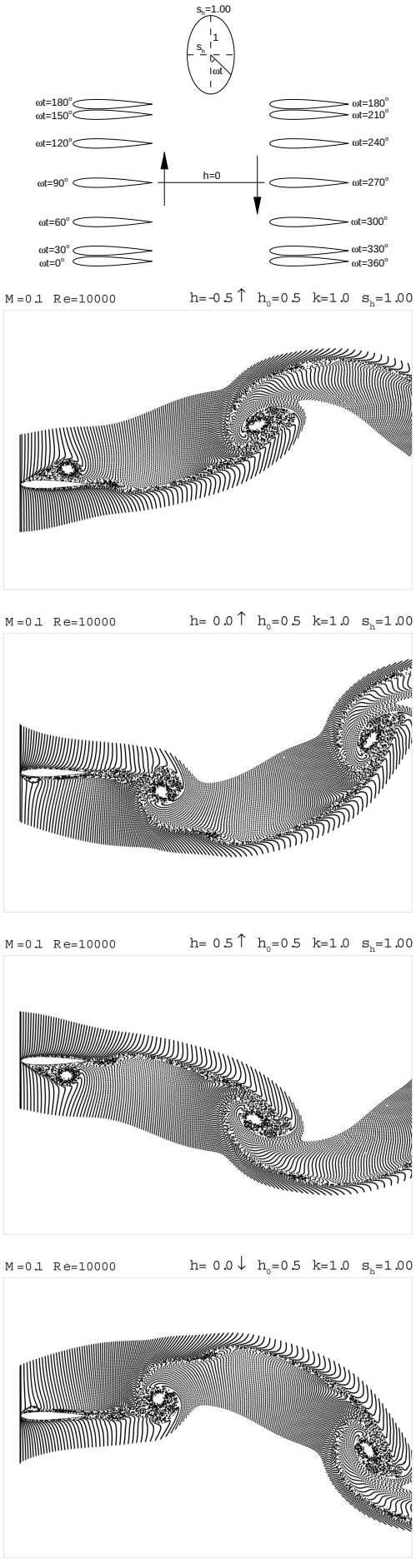


Figure 6: Plunge motion and flowfield for $s_h = 1.0$

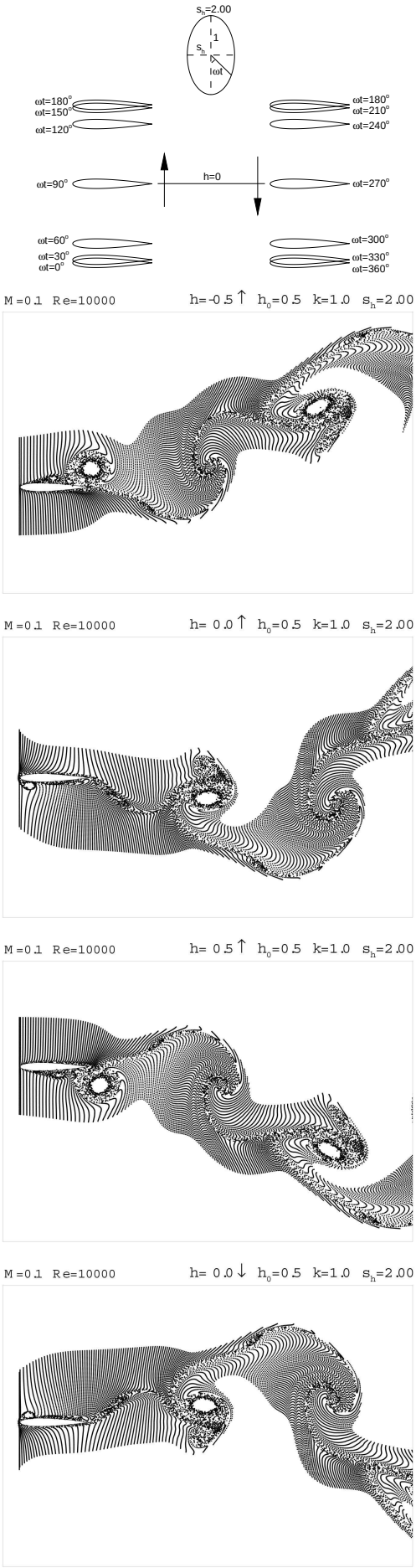


Figure 7: Plunge motion and the flowfield for $s_h = 2.0$

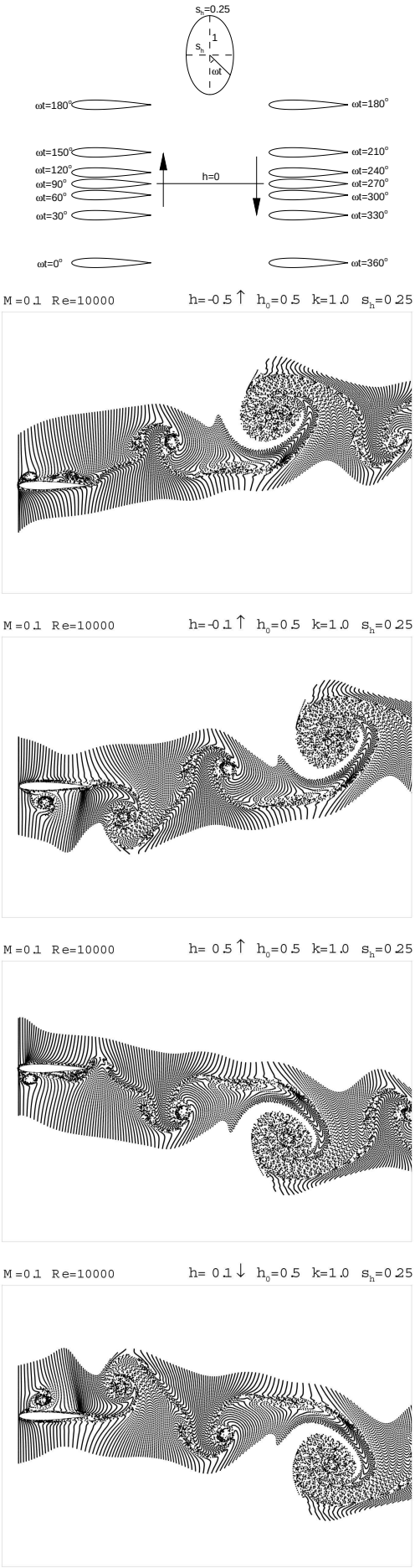


Figure 8: Plunge motion and the flowfield for $s_h = 0.25$

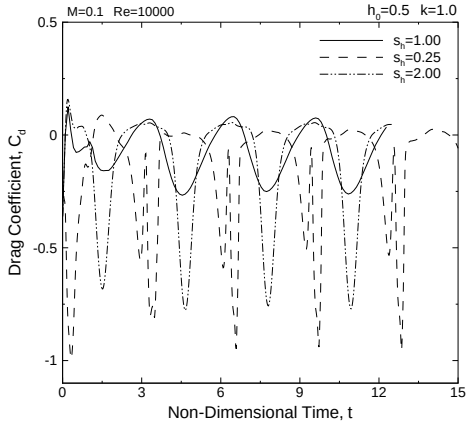


Figure 9: Time variation of drag as a function of $s_h$

In the case $s_h = 0.25$ (Figure 8), where the airfoil reaches high plunge velocities at the minimum and maximum plunge positions, the leading edge vortices follow a completely different trajectory. As observed in the particle traces, the formation of the leading edge vortex on the upper surface is delayed, and as the airfoil starts its upstroke, the vortex is now forced to go over the leading edge down to the lower surface, and convects downstream. The same behavior is observed during the downstroke, which is not shown.

Figure 9 shows the time variation of the drag/thrust coefficient for a few periods of the flapping motion. As seen, a periodic behavior develops along flapping periods. The maximum thrust (minimum drag) values for $s_h = 2.0$ and $s_h = 0.25$ cases are observed to be higher than those for $sh = 1.0$ case. Considering the plunge velocities shown in Figure 4, higher thrust values are associated with the high instantaneous plunge velocities and the resulting suction pressures created at the leading edge [19]. The double dip in the drag coefficient for $s_h = 0.25$ is attributed to the passage of the vortex over the leading edge.

Table 1: Optimization cases and variables

| Case | $\beta$ | $h_0$ | $k$ | $\alpha_0(^o)$ | $s_\alpha$ | $s_h$ | $\phi(^o)$ |
|---|---|---|---|---|---|---|---|
| **1** | 0.0 | 0.5 | 1.0 | $V$ | 1.0 | $V$ | $V$ |
| **2a** | 0.0 | 0.5 | 1.0 | 5.0 | $V$ | $V$ | $V$ |
| **2b** | 0.0 | 0.5 | 1.0 | 5.0 | $V$ | $V$ | $V$ |
| **3** | 0.0 | 0.5 | 1.0 | 10.0 | $V$ | $V$ | $V$ |
| **4** | 0.5 | 0.5 | 1.0 | $V$ | 1.0 | $V$ | $V$ |
| **5** | 1.0 | 0.5 | 1.0 | $V$ | 1.0 | $V$ | $V$ |

### Optimization Study

Optimization studies are performed on an airfoil flapping in combined plunge and pitch. Table 1 summarizes the optimization cases studied. $V$ denotes the optimization variables used in the case study. In Cases 1-3, the objective function is taken to be the average thrust coefficient($\beta = 0.0$). In Case 4, the average thrust coefficient and the propulsive efficiency are given equal weights($\beta = 0.5$). The last optimization Case 4 is performed for maximizing propulsive efficiency($\beta = 1.0$). In Case 2, there are two different starting points for optimization, $a$ and $b$. Corresponding optimization processes for sinusoidally flapping motions ($s_h = 1.0$ and $s_\alpha = 1.0$) are also performed to see the effect of the flatness coefficient. Our numerical experimentation showed that $s_h$ and $s_\alpha$ values greater than $5.0$ and less than $0.2$ produced convergence problems in the solver due to large accelerations of plunge and pitch motions. Therefore, in the optimization studies, $s_h$ and $s_\alpha$ are constrained within the range $0.2 - 5.0$. In all the optimization cases, parallel computations take about $20 - 30$ hours of wall clock time using $4 - 8$ processors.

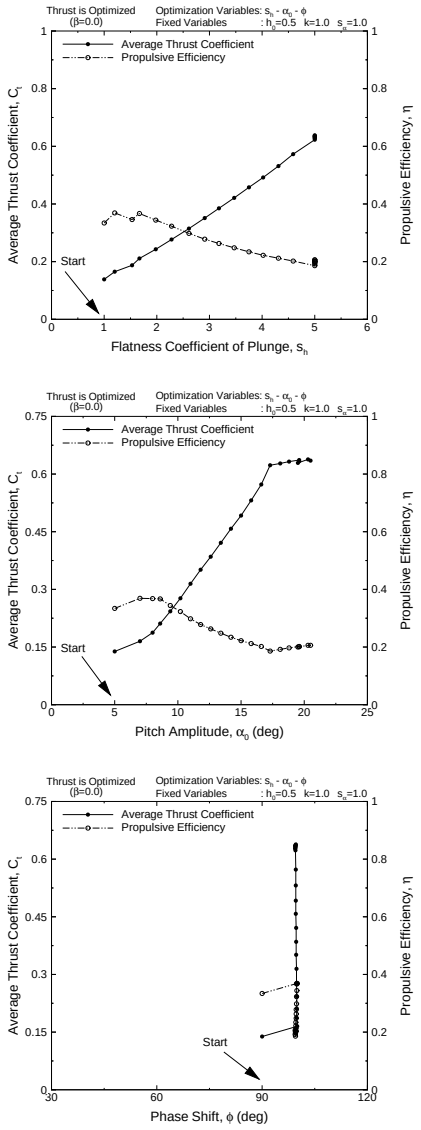


Figure 10: Optimization steps for Case 1

The full path of the optimization process of Case 1 is given in Figure 10. The initial guesses for the optimization are based on our previous experiments. As shown, as the optimization variables are incremented along the gradient of the objective function, the average thrust coefficient increases gradually, and a maximum value of $C_t = 0.638$ is reached at $s_h = 5.0$, $\alpha_0 = 20.3^o$ and $\phi = 99.6^o$. The corresponding propulsive efficiency is $20.6\%$. Starting points

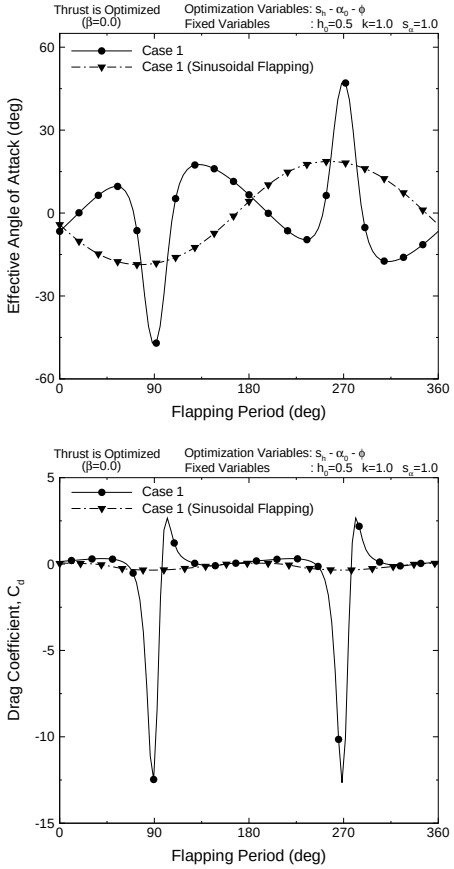


Figure 11: Effective angle of attack variation and unsteady drag/thrust coefficient for Case 1

and results of all the optimization cases are given in Table 2. An optimization process for sinusoidal flapping with variables $\alpha_0$ and $\phi$ provides a much lower average thrust coefficient of $C_t = 0.144$, and twice higher efficiency of $\eta = 42.5\%$ at $\alpha_0 = 8.3^o$ and $\phi = 89.8^o$. It should be noted that the flatness coefficient for plunging motion, $s_h = 5.0$, increases the thrust $4$ times at the expense of reduced efficiency. Effective angle of attack and drag(-thrust) along a period of the optimum motion for Case 1 and the corresponding sinusoidal plunge are shown in Figure 11. In agreement with the previous studies[3, 4], the maximum effective angle of attack occurs around mid-plunge locations which is also the instant when the thrust is maximum. Note that the maximum effective angle of attack for Case 1 is about 3 times greater, and its duration is shorter than that of sinusoidal flapping.

Instantaneous particle traces along the upstroke in a period of the optimized flapping motion for Case 1, and the motion is given in Figure 12. It is clearly seen that the flowfield is highly vortical with strong leading edge vortices. It can be concluded that the high suction induced over the airfoil chord is responsible for the maximum thrust. It should be noted that, the airfoil stays longer at the minimum and maximum plunge positions than it does in a sinusoidal plunging.

In Cases 2 and 3, the flatness coefficient of pitch, $s_\alpha$, is included into the set of optimization variables whereas the pitch amplitude is kept fixed at $\alpha_0 = 5.0$ and $10.0$ degrees

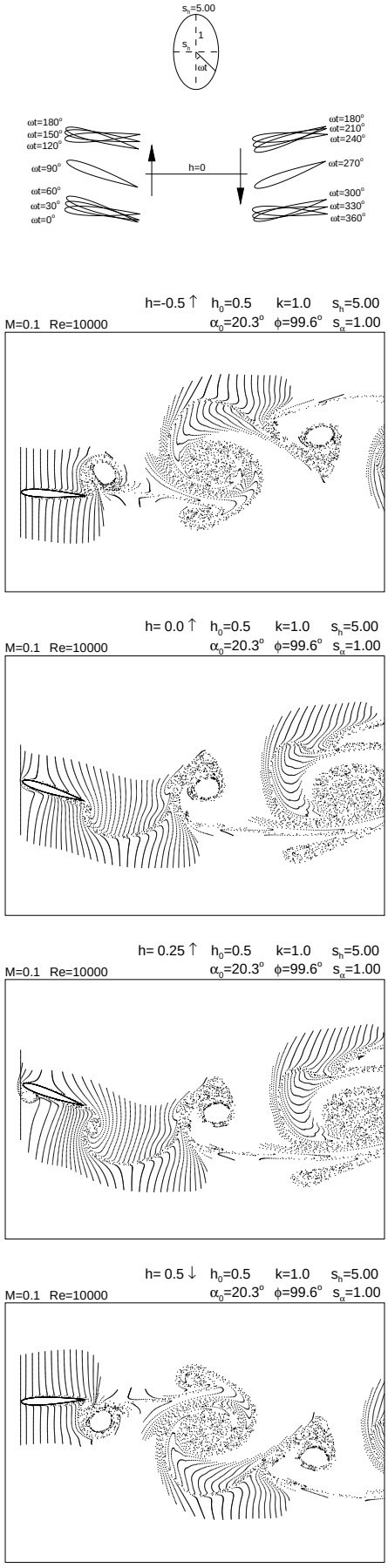


Figure 12: Optimized flapping motion and the flowfield for Case 1

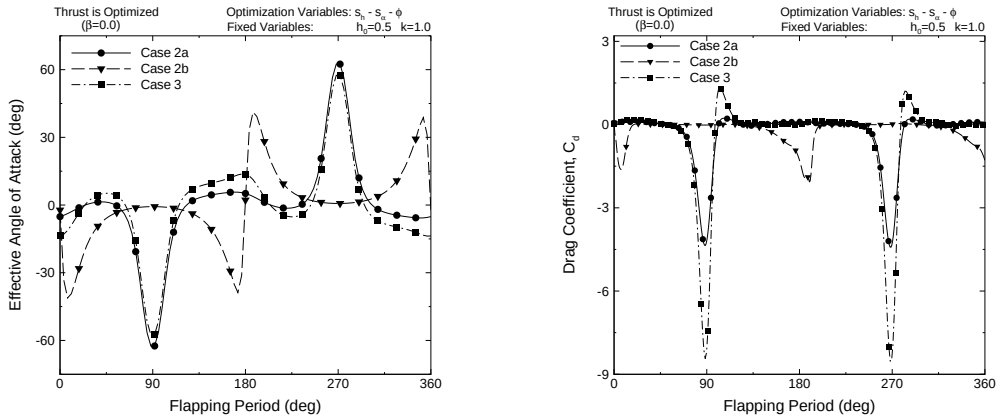


Figure 13: Effective angle of attack variation and unsteady drag/thrust coefficient for Cases 2 and 3

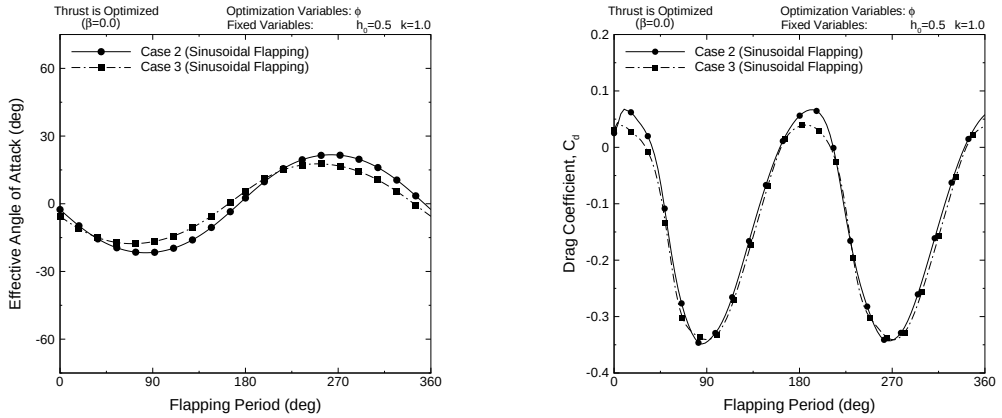


Figure 14: Effective angle of attack variation and unsteady drag/thrust coefficient for Cases 2 and 3 with sinusoidal plunging and pitching

in order to isolate the effects of flatness coefficients. For $\alpha_0 = 5^o$, there are two distinct starting points for plunge and pitch flatness coefficients. $s_h$ and $s_\alpha$ are both initially equal to $1.0$ for case $2a$, and equal to $0.5$ for case $2b$. It is interesting that the plunge flatness coefficient starting from $s_h = 1.0$ converges to the constraint $s_h = 5.0$ while the initial guess of $s_h = 0.5$ leads to the convergence of $s_h = 0.2$ which is the other constraint. The flatness coefficient for pitching has also an interesting convergence. The optimization process commencing with $s_\alpha = 1.0$ ends at $s_\alpha = 2.0$ whereas $s_\alpha$ starting from $0.5$, converges to the constraint $s_\alpha = 5.0$. It seems that high $s_h$ values are associated with low $s_\alpha$ values whereas low $s_h$ occurs if $s_\alpha$ is high. However, the optimized motion in Case 2a with higher $s_h$ and lower $s_\alpha$ provides a higher thrust of $C_t = 0.399$ with a lower efficiency of $\eta = 9.50\%$ than the optimized motion in Case 2b in which the thrust is, $C_t = 0.261$, and the propulsive efficiency is, $\eta = 21.8\%$. As $s_h$ increases, the thrust increases but the efficiency drops. The optimized variables of Case 3, for which the pitch amplitude is now set $\alpha_0 = 10^o$, are close to those of Case 2a(Table 2). It may be concluded that flatness coefficients, $s_h$ and $s_\alpha$ are no very sensitive to $\alpha_0$.

The variation of effective angle of attack and unsteady drag coefficient along a flapping period are given in Figure 13 for Cases 2 and 3. Figure 14 shows the corresponding optimized effective angle of attack and drag history for sinusoidal flapping. In spite of the fact that the pitch amplitude for Case 2 is half of that for Case 3, as observed from Figure 13, Case 2a and 3 give a similar variation of effective angle of attack along a flapping period. The computed average thrust and propulsive efficiency values of these cases are also close to each other. Effective angle of attack seems to be a well defined parameter to estimate the thrust and efficiency of flapping airfoils. There are two instants of maximum effective angle of attack during a flapping stroke for Case 2b since the flatness coefficient for plunging is $s_h = 0.2$. Effective angle of attack variation of the optimized sinusoidal flapping at $\alpha_0 = 5.0^o$ and $\alpha_0 = 10.0^o$ are similar as seen from Figure 14. In Case 2b, the maximum thrust occurs near maximum and minimum plunge positions where the effective angle of attack is maximum.

The previous optimization cases showed that the thrust is maximized at relatively low efficiencies. An optimization process to optimize both the thrust and the efficiency is performed in Case 4. The objective function is a linear combination of the average thrust coefficient and the propulsive efficiency with equal weights. The optimized flapping motion (Table 2) results in $C_t = 0.264$ and $\eta = 42\%$ whereas the optimized sinusoidal flapping motion produces higher efficiency at a low thrust value.

Table 2: Starting points and results of optimization cases

| Case | Starting Conditions | | | | Motion based on the Elliptic Path | | | | | | Sinusoidal Flapping | | | |
|---|---|---|---|---|---|---|---|---|---|---|---|---|---|---|
| | $\alpha_0(^o)$ | $s_\alpha$ | $s_h$ | $\phi(^o)$ | $\alpha_0(^o)$ | $s_\alpha$ | $s_h$ | $\phi(^o)$ | $\mathbf{C_t}$ | $\eta[\%]$ | $\alpha_0(^o)$ | $\phi(^o)$ | $\mathbf{C_t}$ | $\eta[\%]$ |
| **1** | 5.00 | 1.0 | 1.0 | 90.0 | 20.3 | 1.0 | 5.0 | 99.6 | **0.64** | 21 | 8.34 | 89.8 | **0.15** | 43 |
| **2a** | 5.00 | 1.0 | 1.0 | 90.0 | 5.00 | 2.0 | 5.0 | 88.7 | **0.40** | 9.5 | 5.00 | 89.3 | **0.13** | 32 |
| **2b** | 5.00 | 0.5 | 0.5 | 90.0 | 5.00 | 5.0 | 0.2 | 99.9 | **0.26** | 22 | | | | |
| **3** | 10.0 | 2.5 | 1.0 | 90.0 | 10.0 | 2.5 | 5.0 | 85.2 | **0.51** | 13 | 10.0 | 86.7 | **0.15** | 48 |
| **4** | 5.00 | 1.0 | 1.0 | 90.0 | 13.7 | 1.0 | 2.1 | 96.2 | **0.26** | **42** | 12.1 | 84.6 | **0.14** | **53** |
| **5** | 5.00 | 1.0 | 1.0 | 90.0 | 21.9 | 1.0 | 1.0 | 91.0 | 0.078 | **64** | 20.7 | 80.9 | 0.083 | **62** |

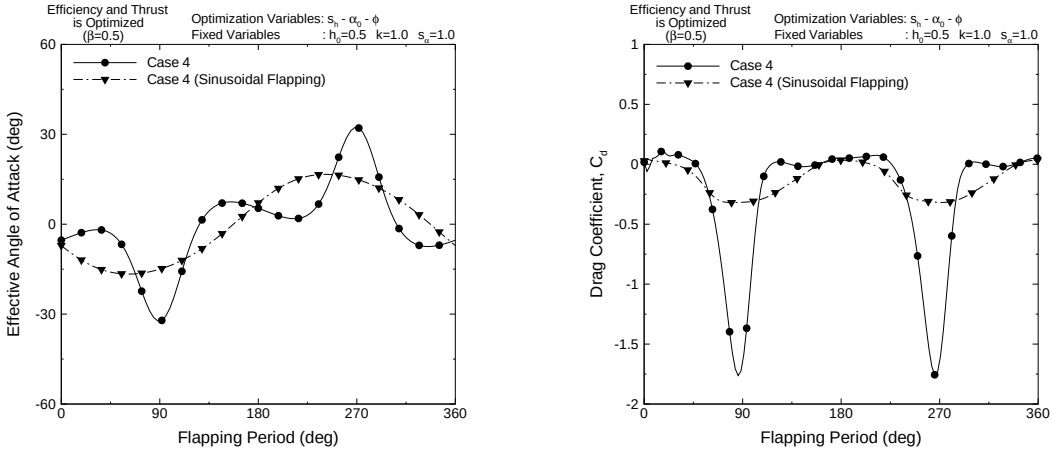


Figure 15: Effective angle of attack variation and unsteady drag/thrust coefficient for Case 4

Similar to Cases 1-3, the flatness coefficient of plunge enhances the thrust generation significantly. Figure 16 shows the optimized flowfield and the flapping motion for Case 4. The formation of the leading edge vortices when the airfoils passes from $h = 0.0$ is seen in the figure. However, the flowfield is observed to be less vortical than in Case 1. Figure 15 gives the effective angle of attack variation and the unsteady drag history. Like in Case 1, the maximum effective angle of attack happens during a short duration at the mid-plunge position. For sinusoidal flapping, the maximum effective angle of attack occurs slightly earlier than the mid-plunge instant.

The objective function in Case 5 is the propulsive efficiency. An interesting convergence is observed in this case(Table 2). Flatness coefficient of plunge, starting from $s_h = 2.0$ converged to about $s_h = 1.1$, which is almost sinusoidal plunging. One may conclude that if pitching is sinusoidal, then, plunging must also be sinusoidal for maximum efficiency. The converged efficiency, $\eta = 64.1\%$, is maximized at the pitch amplitude, $\alpha_0 = 21.9^o$, and at the phase shift, $\phi = 90^o$. The fact that the maximum propulsive efficiency producing optimum phase shift occurs near $\phi = 90^o$ is consistent with previous optimization studies[3, 5, 4] about sinusoidally flapping airfoils. In Figure 17, the instantaneous particle traces of the optimum motion along a flapping period are given. In contrast to the flowfield observation in Cases 1 and 4, the leading edge formation is prevented, which maximizes the propulsive efficiency. The unsteady flow becomes more streamlined with the motion of the airfoil. The corresponding effective angle of attack variation and unsteady drag are given in Figure 18. For an efficient flapping, the effective angle of attack at the mid-plunge location is set about $0\ deg$[4].

Table 2 gives a summary of the optimized flapping motions based on both the elliptic and circular path(sinusoidal motion). As seen from the table, flatness coefficients of plunge and pitch, $s_h$ and $s_\alpha$, provide high enhancement in the thrust generation. Case 4 clearly shows that thrust may be increased without decreasing the propulsive efficiency.

## CONCLUDING REMARKS

A new periodic flapping motion which is based on plunge and pitch flatness coefficients, is introduced to optimize the thrust and propulsive efficiency of flapping airfoils. The optimization of thrust generation and propulsive efficiency together is achieved with a weighted and normalized objective function. Thrust generation of a flapping airfoil is maximized at large flatness coefficients with large leading edge vortices forming and shedding into the wake. The airfoil stays at high effective angle of attacks during short durations in the upstroke and the downstroke. Propulsive efficiency of the flapping airfoils may be increased by reducing the effective angle of attack, and consequently by preventing the formation of leading edge vortices. Further research is in progress to introduce additional parameters in the definition of the flapping motion, and to optimize the thrust generation of flapping airfoils.

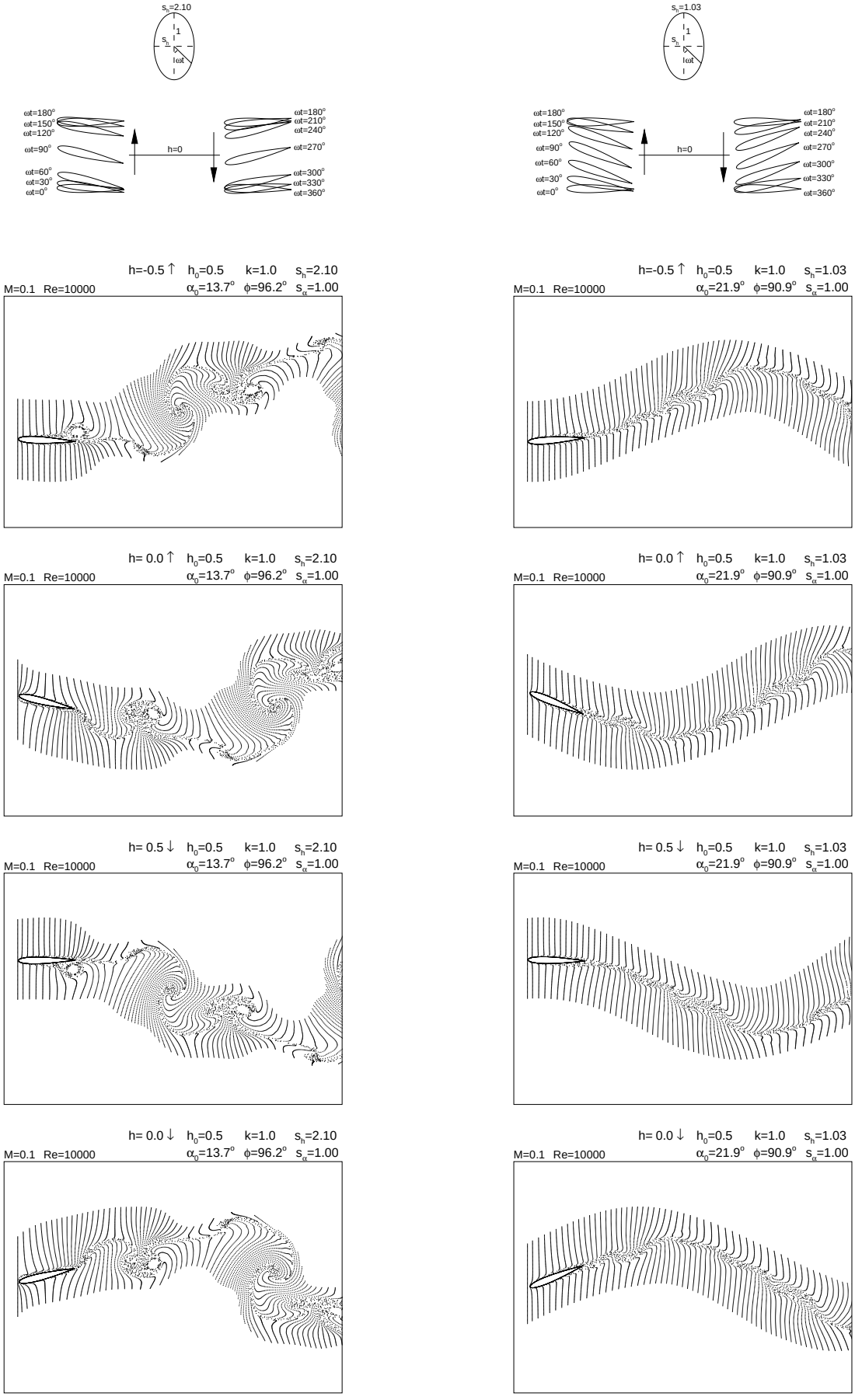


Figure 16: Optimized flapping motion and the flowfield for Case 4

Figure 17: Optimized flapping motion and the flowfield for Case 5

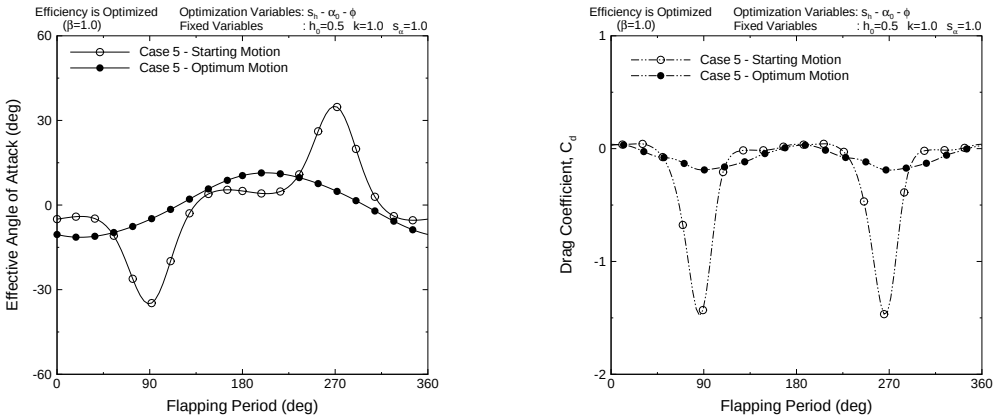


Figure 18: Effective angle of attack variation and unsteady drag/thrust coefficient for Case 5

# References


[1] Kurtulus, D. F., Farcy, A. and Alemdaroglu, N., *Unsteady Aerodynamics of Flapping Airfoil in Hovering Flight at Low Reynolds Numbers*, $43^{rd}$ AIAA Aerospace Sciences Meeting and Exhibit, Reno, NV, Jan 2005.

[2] Dong, H., Mittal, Bozkurttas, M., R. and Najjar, F., *Wake Structure and Performance of Finite Aspect-Ratio Flapping Foils*, $43^{rd}$ AIAA Aerospace Sciences Meeting and Exhibit, Reno, NV, Jan 2005.

[3] Kaya, M., *Computation of Viscous Flows Over Flapping Airfoils and Parallel Optimization of Flapping Parameters*, Msc. Thesis, METU, 2003.

[4] Tuncer, I.H. and Kaya, M., *Optimization of Flapping Airfoils For Maximum Thrust and Propulsive Efficiency*, $3^{rd}$ Int. Conference on Advanced Engineering Design, Prague, Czech Republic, June 1-5 2003.

[5] Tuncer, I.H. and Kaya, M., *Optimization of Flapping Airfoils for Maximum Thrust*, AIAA Paper, No 2003-0420, Jan 2003.

[6] Jones, K.D. and Platzer, M.F., *Experimental Investigation of the Aerodynamic Characteristics of Flapping-Wing Micro Air Vehicles*, AIAA Paper, No 2003-0418, Jan 2003.

[7] Jones, K.D., Castro, B.M., Mahmoud, O., Pollard, S.J., Platzer, M.F., Neef, M.F., Gonet, K., Hummel, D. *A Collaborative Numerical and Experimental Investigation of Flapping-Wing Propulsion*, AIAA Paper, No 2002-0706, Jan 2002.

[8] Jones, K.D., Duggan, S.J., Platzer, M.F., *Flapping-Wing Propulsion for a Micro Air Vehicle*, AIAA Paper, No 2001-0126, Jan 2001.

[9] Mueller, T.J. (editor), *Fixed and Flapping Wing Aerodynamics for Micro Air Vehicles*, AIAA Progress in Aeronautics and Astronautics, Vol 195, Reston, VA, 2001.

[10] Isogai, K. and Shinmoto Y., *Study on Aerodynamic Mechanism of Hovering Insects*, AIAA Paper, No 2001-2470, 2001.

[11] Tuncer, I.H. and Platzer, M.F., *Computational Study of Flapping Airfoil Aerodynamics*, AIAA Journal of Aircraft, Vol 35, p: 554-560, 2000.

[12] Platzer, M.F. and Jones, K.D., *The Unsteady Aerodynamics of Flapping-Foil Propellers*, $9^{th}$ International Symposium on Unsteady Aerodynamics, Aeroacoustics and Aeroelasticity of Turbomachines, Ecole Centrale de Lyon, Lyon, France, Sept 2000.

[13] Isogai, K., Shinmoto Y., Watanabe, Y., *Effects of Dynamic Stall on Propulsive Efficiency and Thrust of a Flapping Airfoil*, AIAA Journal, Vol 37, p: 1145-1151, 2000.

[14] Shyy, W., Berg, M. and Lyungvist, D., *Flapping and Flexible Wings for Biological and Micro Air Vehocles*, Pergamon Progress in Aerospace Sciences, Vol 35, p: 455-505, 1999.

[15] Lai, J.C.S. and Platzer, M.F., *The Jet Characteristics of a Plunging Airfoil*, $36^{th}$ AIAA Aerospace Sciences Meeting and Exhibit, Reno, NV, Jan 1998.

[16] Jones, K.D., Dohring, C.M. and Platzer, M.F., *An Experimental and Computational Investigation of the Knoller-Beltz Effect*, AIAA Journal, Vol 36, p: 1240-1246, 1998.

[17] Anderson, J.M., Streitlen, K., Barrett, D.S. and Triantafyllou, M.S., *Oscillating Foils of High Propulsive Efficiency*, Journal of Fluid Mechanics, Vol 360, p: 41-72, 1998.

[18] Tuncer, I.H., Lai, J., Ortiz, M.A, and Platzer, M.F., *Unsteady Aerodynamics of Stationary/Flapping Airfoil Combination in Tandem*, AIAA Paper, No 97-0659, 1997.

[19] Tuncer, I.H. and Platzer, M.F., *Thrust Generation due to Airfoil Flapping*, AIAA Journal, Vol 34, p: 324-331, 1995.